scientific reports

Check for updates

OPEN

Periodic switching of acoustic radiation force with beat created by multitone field

Hiroya Tanaka✉, Keita Funayama & Yukihiro Tadokoro

Acoustic radiation force plays a key role in microfluidic systems for particle and cell manipulation. In this study, we investigate the acoustic radiation force resulting from synthesized ultrasounds that are emitted from multiple sound sources with slightly different oscillation frequencies. Due to the synthesized field, the acoustic radiation force is expressed as the sum of a dc component and harmonics of fundamental frequencies of a few hertz. This induces the beat of the acoustic radiation force. We demonstrate that the synthesized field provides the periodic on/off switching of the acoustic radiation force associated with the one denominational planar standing wave in a straight microfluidic channel. Consequently, our system can temporally manipulate acoustic radiation force without active controls.

Acoustic radiation force is a widely studied topic and continues to generate interest in fields ranging from simple dynamics[1–3] to the broad applications such as acoustic levitators[4–6], tweezers[7,8], and displays[9,10]. In addition, recent developments in microfabrication technologies have enabled the integration of ultrasound transducers in the microfluidic systems, which has led to further interest in acoustic radiation force[11]. Acoustic radiation force realizes contact-free particle and cell manipulations such as concentration[12,13], trapping[14,15], and separation[16–18], based on their acoustomechanical properties.

Acoustic radiation force is induced by the scattering of the acoustic waves on a small particle[19–22]. The observed motion of the small particle is not resolved on the time scale of kHz/MHz ultrasound waves[23,24]. Consequently, acoustophoretic motion is generated by the force averaged over the oscillation cycle. When the monotone acoustic wave is incident on the small particle, the scattering of acoustic waves gives rise to the time-invariant force in steady microfluidic channels.

However, recent studies have analyzed the time dependency of acoustophoretic motion. For example, the oscillating sharp-edge structure attracts or repels the particles in the microfluidic channel over a period of several seconds[25]. Meanwhile, it has been demonstrated that short acoustic pulses can increase the acoustic trapping selectivity[26,27]. Two denominational patterns of the acoustic radiation force are obtained by tuning the transient acoustic fields. Furthermore, experiments have shown that two mutually interfering acoustic fields yield amplitude modulation over time[28]. A slight frequency difference between the acoustic fields leads to a slow phase shift and causes a local rotation of the nodal pressure for the particle clumps in the fluidic chamber.

In this study, we theoretically analyze the time dependency of the acoustic radiation force at a slow time scale of several seconds when multiple ultrasounds are simultaneously incident on a small spherical particle. The synthesized ultrasounds are emitted from multiple sound sources with marginally different frequencies. To capture the dynamics, we separate the time scale into fast (∼ time period of ultrasound oscillation) and slow (∼ a few seconds). Subsequently, the acoustic radiation force at the slow time scale is expressed as the sum of the time-invariant component and the harmonics of the fundamental angular frequency of a few Hz. This indicates that the response of the acoustic radiation force in time can be controlled with multiple sources without active controls. To provide an instance of this control, we experimentally demonstrate that the synthesized field allows for the periodic on/off switching of the acoustic radiation force for one denominational planar standing wave in the straight microfluidic channel. In addition, we analyze the tunability of time response in terms of the amplitude of the harmonics.

Typically, studies have discussed the acoustic radiation force in the monotone field oscillating with the specific frequency. The monotone field induces a time-invariant acoustic radiation force, unlike the multitone field that induces a fluctuating or time-variant radiation force. This time-variant force comes from down-converted harmonic series, which serves as the beat of the acoustic radiation force. We rigorously analyze the beat of the
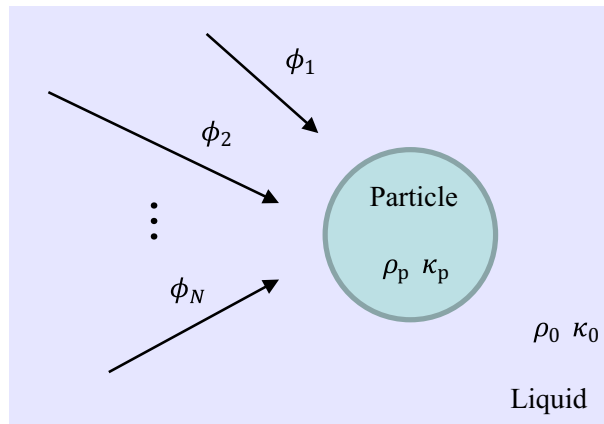
nature portfolio

1

Figure 1. Schematic of the analytical model. Multiple incoming acoustic waves with potentials, $\phi_1, \ldots, \phi_N$, of the different angular frequency, $\omega_1, \ldots, \omega_N$, are incident on a small compressible spherical particle of compressibility κ_p and density ρ_p. Such acoustic waves are synthesized in space and scatter at the particle surface. The particle is surrounded by the compressible inviscid bulk fluid of compressibility κ_0 and density ρ_0.

acoustic radiation force based on the general theoretical model. Moreover, our approach reveals the methodology for the manipulation of the acoustic radiation force over a period without active controls.

For the active control over time, the acoustic radiation force should be adaptively strengthened by tuning the voltage applied to the sound transducers. Adaptive voltage control requires complex integrated circuits with surrounding components, increasing the system size. However, our system provides a method for temporal manipulation of the acoustic radiation force without active control and complex circuity. Thus, our manipulation methodology reduces the system sizes in programmable microfluidic channels.

Results

The model.   We focus on a spherical particle in the microfluidic channels and analyze the acoustic radiation force resulting from the scattering of the acoustic waves by the particle. Figure 1 illustrates the concept of our analysis. We impose an ultrasound field on the fluid containing small particles that are significantly smaller than the ultrasound wavelength. Assuming that the fluid is inviscid and incomprehensive, we consider the fluid motion in linear approximation. The corresponding Navier–Stokes equations are

$$\frac{\partial \rho}{\partial t} + \rho_0 \nabla \cdot \boldsymbol{v} = 0, \tag{1}$$

$$\frac{\partial \boldsymbol{v}}{\partial t} + \frac{1}{\rho_0} \nabla p = 0, \tag{2}$$

where ρ is the fluid density, ρ_0 is the equilibrium fluid density, $\boldsymbol{v}$ is the fluid velocity, $p = c_0^2 \rho$ is the fluid pressure, and c_0 is the speed on the sound in the fluid.

According to Gor'kov's theory[3], the acoustic radiation force acting on the small particle is expressed as

$$\boldsymbol{F}(\boldsymbol{r}, t) = -\frac{4\pi}{3} a^3 \nabla \left[\frac{1}{2} \mathrm{Re}[f_1] \kappa_0 \langle p^2 \rangle - \frac{3}{4} \mathrm{Re}[f_2] \rho_0 \langle v^2 \rangle \right], \tag{3}$$

where a is the particle radius, $f_1 = 1 - \kappa_p/\kappa_0$, $f_2 = 2(\rho_p - \rho_0)/(2\rho_p + \rho_0)$, κ_0 (or κ_p) is the comprehensibility of the fluid (or particle), ρ_p is the equilibrium density of the particle, $v = |\boldsymbol{v}|$ is the absolute value of the velocity, and the notation $\mathrm{Re}[\cdot]$ is the real part of the complex variable. The notation $\langle x \rangle$ is the time average over an oscillation period τ:

$$\langle x \rangle \equiv \frac{1}{\tau} \int_0^\tau x \, \mathrm{d}t. \tag{4}$$

Introducing the velocity potential ϕ, the pressure and velocity are calculated by $p = -\rho_0(\partial \phi/\partial t)$ and $\boldsymbol{v} = \nabla \phi$. It should be noted that the force $\boldsymbol{F}(\boldsymbol{r}, t)$ is a function of the spatial coordinate $\boldsymbol{r}$ and time t.

Here, we introduce incident acoustic waves from multiple sound sources, see Fig. 1. Then, we have the time-varying multitone field:

$$\phi = \sum_{n=1}^{N} \phi_n \cos(\omega_n t + \theta_n), \tag{5}$$

with amplitude $\{\phi_1, \ldots, \phi_N\}$, angular frequency $\{\omega_1, \ldots, \omega_N\}$, and relative phase $\{\theta_1, \ldots, \theta_N\}$. The pressure and velocity are expressed as

$$p = \sum_{n=1}^{N} p_n \sin(\omega_n t + \theta_n), \tag{6}$$

$$\boldsymbol{v} = \sum_{n=1}^{N} \boldsymbol{v}_n \cos(\omega_n t + \theta_n), \tag{7}$$

where $p_n = \rho_0 \phi_n \omega_n$ and $\boldsymbol{v}_n = \boldsymbol{\nabla} \phi_n$.

From Eqs. (6) and (7), the time average of the squared-pressure and velocity are written as

$$\langle p^2 \rangle = \left\langle \sum_{m=1}^{M} \sum_{n=1}^{N} \left(-\frac{p_m p_n}{2} \right) \cos[(\omega_m + \omega_n)t + \theta_m + \theta_n] + \sum_{m=1}^{M} \sum_{n=1}^{N} \frac{p_m p_n}{2} \cos[(\omega_m - \omega_n)t + \theta_m - \theta_n] \right\rangle, \tag{8}$$

$$\langle v^2 \rangle = \left\langle \sum_{m=1}^{M} \sum_{n=1}^{N} \frac{\boldsymbol{v}_m \cdot \boldsymbol{v}_n}{2} \cos[(\omega_m + \omega_n)t + \theta_m + \theta_n] + \sum_{m=1}^{M} \sum_{n=1}^{N} \frac{\boldsymbol{v}_m \cdot \boldsymbol{v}_n}{2} \cos[(\omega_m - \omega_n)t + \theta_m - \theta_n] \right\rangle. \tag{9}$$

We now assume a marginal frequency discrepancy in the synthesized fields, i.e., $\omega_n = \omega_0 + (n-1)\delta\omega$ and $\delta\omega \ll \omega_0$. Thus, we can distribute the time scale between the dynamics of the fast and slow time scales in Eqs. (8) and (9). The first terms describing the fast oscillation become zero in the time average operation because the acoustophoretic motion does not have the resolution on the millisecond/microsecond time scale of kHz/MHz ultrasound waves. More specifically, we have $\langle \cos[\{2\omega_0 + (m+n-2)\delta\omega\}t + \theta_m + \theta_n] \rangle = 0$. In contrast, the second terms take nonzero value in the time average since it varies in slow time scale compared to the oscillation cycle, i.e., $2\pi/\delta\omega \gg \tau$. Therefore, we can rewrite Eqs. (8) and (9) as

$$\langle p^2 \rangle = \sum_{m=1}^{M} \sum_{n=1}^{N} \frac{p_m p_n}{2} \cos[(m-n)\delta\omega t + \theta_m - \theta_n], \tag{10}$$

$$\langle v^2 \rangle = \sum_{m=1}^{M} \sum_{n=1}^{N} \frac{\boldsymbol{v}_m \cdot \boldsymbol{v}_n}{2} \cos[(m-n)\delta\omega t + \theta_m - \theta_n]. \tag{11}$$

When we assume the quantized relative phase $\theta_n - \theta_m \in [0, \pi]$, we can introduce the sign function, $s_{j,i+j}$. Substituting Eqs. (10) and (11) to Eq. (3), we have

$$\boldsymbol{F}(\boldsymbol{r}, t) = \sum_{i=0}^{N-1} \boldsymbol{F}_i(\boldsymbol{r}) \cos(i\delta\omega t), \tag{12}$$

where

$$\boldsymbol{F}_i(\boldsymbol{r}) = -\frac{4\pi}{3} a^3 \boldsymbol{\nabla} \left[\frac{1}{2} \mathrm{Re}[f_1] \kappa_0 \frac{f_i^{(\mathrm{p})}}{2} - \frac{3}{4} \mathrm{Re}[f_2] \rho_0 \frac{f_i^{(\mathrm{v})}}{2} \right], \tag{13}$$

$$f_i^{(\mathrm{p})} = \sum_{j=1}^{N-i} s_{j,i+j} \alpha_i p_j p_{i+j}, \tag{14}$$

$$f_i^{(\mathrm{v})} = \sum_{j=1}^{N-i} s_{j,i+j} \alpha_i \boldsymbol{v}_j \cdot \boldsymbol{v}_{i+j}, \tag{15}$$

$$s_{j,i+j} = \begin{cases} 1 & \text{if } \theta_j - \theta_{i+j} = 0 \\ -1 & \text{if } \theta_j - \theta_{i+j} = \pm\pi \end{cases}, \tag{16}$$

$$\alpha_i = \begin{cases} 1 & \text{if } i = 0 \\ 2 & \text{if } i \geq 1 \end{cases}. \tag{17}$$

It should be noted that the function $\boldsymbol{F}_i(\boldsymbol{r})$ specifies the spatial distributions of the magnitude of the acoustic radiation force. In addition, this distribution varies in time resulting from the harmonics $\cos(i\delta\omega t)$ at the fundamental angular frequency $\delta\omega$.
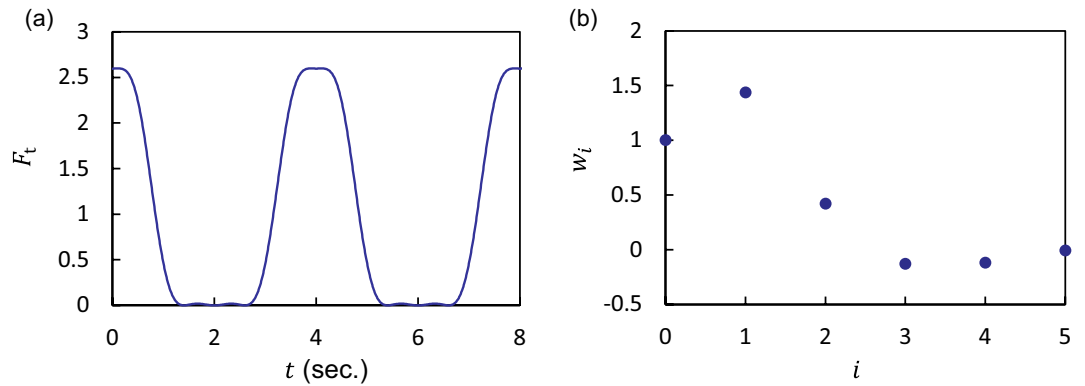
Figure 2. (**a**) Variation in time of F_t, which is designed to be periodically switched acoustic radiation force. (**b**) Weight w_i, allowing for the periodic switch. We set the frequency differential to $\delta\omega/(2\pi) = 0.25$ Hz and the number of the incident waves to $N = 6$. The amplitudes are $\tilde{p}_1 = 0.02854$, $\tilde{p}_2 = 0.4314$, $\tilde{p}_3 = 0.72149$, $\tilde{p}_4 = 0.51841$, $\tilde{p}_5 = 0.05564$, and $\tilde{p}_6 = 0.14385$. The phases are $\theta_1 = \cdots = \theta_5 = 0$ and $\theta_6 = \pi$.

Periodic switching of acoustic radiation force created by one dimensional standing wave. The time response of the acoustic radiation force can be designed according to the amplitudes and relative phases of the incident ultrasounds. Here, we theoretically demonstrate the periodic on/off switching without active controls for an instance of the design of the time response.

We now analyze one dimensional planar standing wave generated by the multitone ultrasound in the straight microfluidic channel. Considering the boundary condition at the side walls of one dimensional channel, we have a synthesized field[24],

$$p = \sum_{n=1}^{N} p_n \cos(kz) \sin(\omega_n t + \theta_n), \tag{18}$$

$$\boldsymbol{v} = \begin{pmatrix} 0 \\ 0 \\ \sum_{n=1}^{N} \left(-\frac{p_n}{\rho_0 c_0} \right) \sin(kz) \cos(\omega_n t + \theta_n) \end{pmatrix}, \tag{19}$$

where $k = 2\pi/\lambda_0 = \omega_0/c_0$, $\lambda_0/2 = l$, and l is the channel width. We assume that the incident waves with each angular frequency $\omega_n (n = 1, \ldots, N)$ creates a similar force distribution, i.e, $\sin(2k_n z) \approx \sin(2kz)$ for $k_n = \omega_n/c_0$ at $n = 1, \ldots, N$.

Substituting Eqs. (18) and (19) to Eq. (3), we have the following relation,

$$F(z, t) = F_z(z) F_t(t), \tag{20}$$

where

$$F_z(z) = 4\pi \Phi k a^3 E \sin(2kz), \tag{21}$$

$$F_t(t) = \sum_{i=0}^{N-1} w_i \cos(i\delta\omega t), \tag{22}$$

$$w_i = \sum_{j=1}^{N-i} s_{j,i+j} \alpha_i \tilde{p}_j \tilde{p}_{i+j}, \tag{23}$$

and $\Phi = f_1/3 + f_2/2$, $E = (\sum_{n=1}^{N} p_n^2)/(4\rho_0 c_0^2)$, and $\tilde{p}_j = p_j/\sqrt{\sum_{n=1}^{N} p_n^2}$. Note that Φ is the the acoustophoretic contrast factor[24], and E is the acoustic energy density.

The force distribution is modulated owing to the multiple incident ultrasounds. When the frequency difference is perceptible (e.g., $\delta\omega/(2\pi)$ is lower than 1 Hz), we observe the change in the acoustic radiation force of the order of a few seconds. We demonstrate the periodic on/off switching of the acoustic radiation force based on the modulated field. Figure 2a shows a numerical example of time response to illustrate the switching behavior at an interval of 4 s. The strength of the field distribution $F_z(z)$ is weighted according to $F_t(t)$. At approximately $t = 0$, 4 s, and 8 s, we have *on state*: $F \approx 2.6 F_z(z)$. At $t = 2$ s and 6 s, we have *off state*, in which we observe the considerably small force: $F \approx 0$. To realize such switching behavior, we used $N = 6$ and the weights $w_0, \ldots, w_5$, as shown in Fig. 2b.
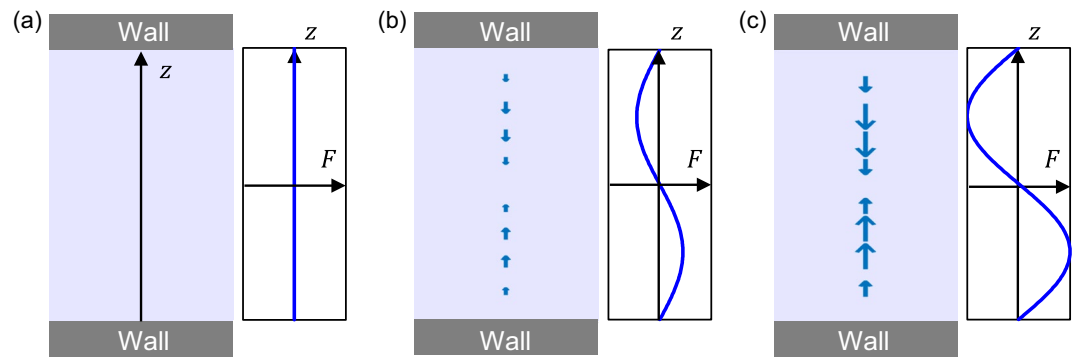
Figure 3. Left panels: cross-section sketches of a straight, hard-walled water-filled channel. The acoustic radiation force is illustrated by blue arrows at time (**a**) $t = 2$ s, (**b**) 3.2 s, and (**c**) 4 s. Right panels: transverse and standing ultrasound wave in the channel.
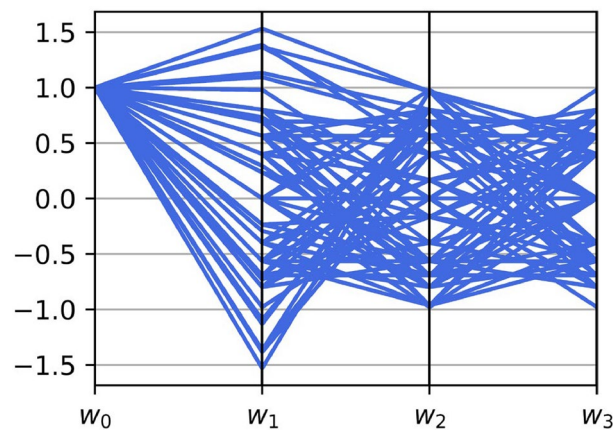

Figure 4. Possible values of the weight w_i at $N = 4$ with the constraint of $\sum_{n=1}^{N} \tilde{p}_n^2 = 1$ on parallel coordinates. The value of $\tilde{p}_i$ for each i is incremented by 0.2.

For further understanding, we illustrate the time variation of the force distribution at $t = 2$ s, 3.2 s, and 4 s in Fig. 3. The acoustic radiation force is periodically turned on and off at specific intervals. Note that the sign of F_z depends on the acoustophoretic contrast factor Φ, i.e., $F_z \propto +\sin(2kz)$ for $\Phi > 0$ and $F_z = -\sin(2kz)$ for $\Phi < 0$[24]. In our study, the contrast factor was assumed to be positive.

The time response of the acoustic radiation force is programmable via the weights provided by the multitone field. To understand the tunability, we plotted the possible weight values at $N = 4$ on the parallel coordinates as shown in Fig. 4. We introduced the constraint $\sum_{n=1}^{N} \tilde{p}_n^2 = 1$ to maintain the acoustic energy density as a constant. Furthermore, we calculated the possible range of w_1 and w_2 for specific values of w_3: (a) $w_3 = 0.1$ and (b) 0.45. From Eq. (23), we plotted the relation between w_1 and w_2 as shown in Fig. 5. The blue-hatched region is the possible range without the constraint on w_3.

Experimental demonstration for periodic switching. We verified the switching behavior through measurements. In the initial setup, the particles were uniformly distributed in the channel. We examined the trajectory of the particles imposed by the synthesized ultrasounds that were periodically switched at an interval of 4 s, see Fig. 2a. Figure 6a shows the deviation in the position of a certain particle with respect to a reference position over time. Moreover, Fig. 6b shows the mean displacement every 1 s for 30 particles. The particles drifted steeply at intervals of approximately four seconds; this drift can be attributed to the periodic drag induced by the restless acoustic radiation force on the particles in the microfluidic channels.

Furthermore, the snapshots of the particle motion from $t = 4$ s to 9 s are shown in Fig. 6c. We observed that the particle moved away from the reference plane (orange dotted line) over time with a significantly steep drift between $t = 6$ s and 8 s. This can be attributed to the switching of the force applied to the particle.

Discussion
The acoustic radiation force is typically discussed in the context of a field that oscillates monotonically with the specific angular frequency, ω_0. Then, substituting $N = 1$ to Eq. (12), the harmonic series is simply written as the single term, $\boldsymbol{F}(\boldsymbol{r}, t) = \boldsymbol{F}_0(\boldsymbol{r})$, due to $\cos(i\delta\omega t) = 1$ at $i = 0$. This indicates that the acoustic radiation force
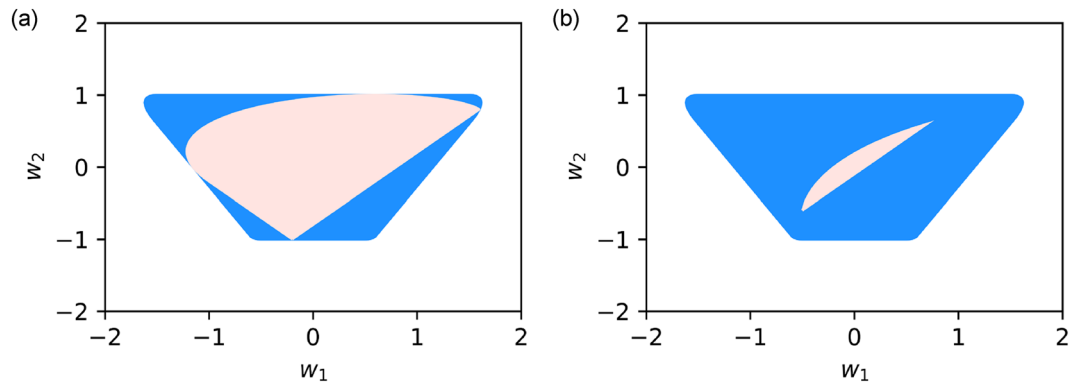
Figure 5. Possible range of the weights w_1 and w_2 at $N = 4$ with the constraint as $\sum_{n=1}^{N} \tilde{p}_n^2 = 1$ and the fixed value of w_3: (**a**) $w_3 = 0.1$ and (**b**) 0.45. This region is filled with bright red. The blue hatched region is the possible range without the constraint on w_4.
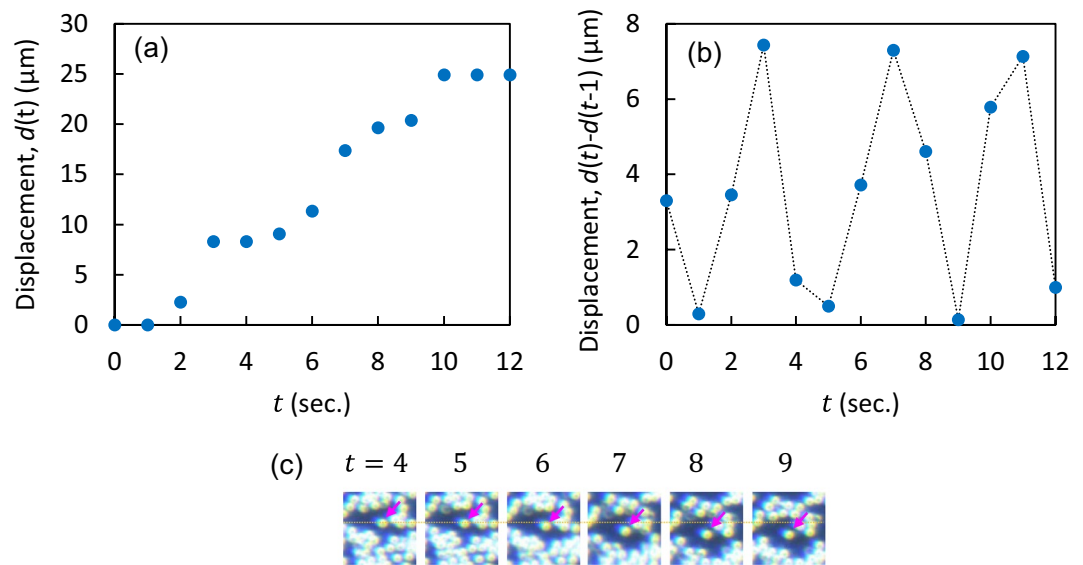

Figure 6. (**a**) Deviation of the position of a certain particle with respect to the reference position at $t = 0$. The displacement is measured from the optical microscope images. (**b**) Mean displacement every 1 s for 30 particles. (**c**) Snapshots of the particle motion in (**a**) for several seconds. Orange dashed line indicates the position at $t = 4$ s. The particle of interest is indicated by the pink arrow.

is independent of time, i.e., it is described as the function of the spatial coordinate, $\boldsymbol{r}$. In contrast, when there are multiple incident fields at $N \geq 2$, the acoustic radiation force is expressed as the sum of harmonics at the fundamental frequency, $\delta\omega$. Furthermore, we observe that the resulting acoustic radiation force is the beat that experiences interference from the time-varying forces with multiple frequencies.

According to Eq. (13), the distribution of the acoustic radiation force varies in time resulting from the harmonics $\cos(i\delta\omega t)$. Thus, the switching period of acoustic radiation force is determined by the frequency difference $\delta\omega$. Specifically, in our analysis, we set the fundamental angular frequency $\delta\omega/(2\pi) = 0.25$ Hz, i.e., the switching period $2\pi/\delta\omega = 4$ s.

Interestingly, the acoustic radiation force is not considered as a superposition of the fields $\phi_1, \ldots, \phi_N$ because it has nonlinear behavior owing to the squaring operation (p^2 and v^2); see Eq. (2). This nonlinear effect leads to the complicated description of the acoustic radiation force in the synthesized field, which is represented as a superposition of the harmonics with the amplitudes $\boldsymbol{F}_0, \ldots, \boldsymbol{F}_{N-1}$.

From the tunability analysis, we see that the steady component takes the constant value: $w_0 = \sum_{n=1}^{N} \tilde{p}_n^2 = 1$, see Fig. 4. The acoustic radiation force created by the synthesized ultrasound includes a time-invariant (steady) component that is the sum of the radiation force created by the monotone fields. In contrast, the weight of the higher-order components, $w_1, \ldots, w_{N-1}$, varies within the specific range.

Moreover, both w_1 and w_2 have a large range of values (i.e., red region in Fig. 5a) when the value of the higher order weight is small, i.e., $w_3 = 0.1$. On the contrary, w_2 and w_3 exist in the narrow region (i.e., red region in Fig. 5b) at $w_3 = 0.45$. This is because the weight is associated with the multivariable polynomial, as shown in
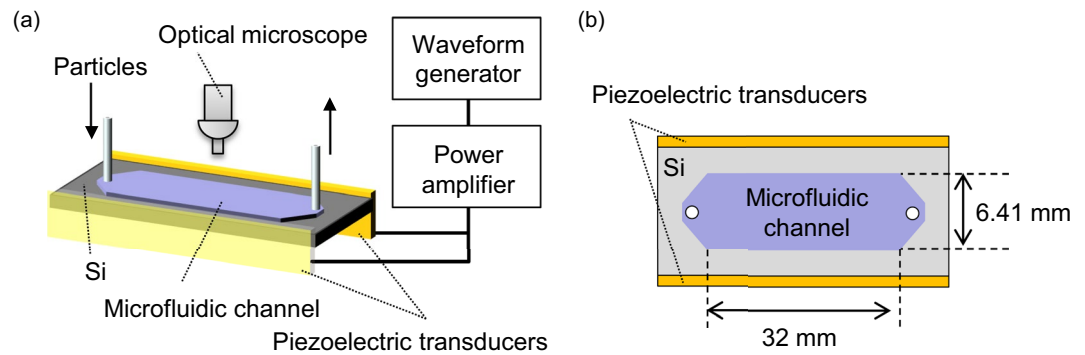
Figure 7. (**a**) Overview of measurement setup. (**b**) Top view of the channel.

Eq. (23). Therefore a large (small) value of w_3 gives rise to the narrow (wide) possible range of w_1 and w_2. From Eq. (23), we also see that the tunability of the lower order weight is more flexible than that of the higher order weight, since it is described using a larger number of variables. For instance, w_1 is the function of $\tilde{p}_1$, $\tilde{p}_2$, $\tilde{p}_3$, and $\tilde{p}_4$ whereas w_3 is that of only $\tilde{p}_1$ and $\tilde{p}_4$ at $N = 4$.

In conclusion, we have demonstrated that the beat of the acoustic radiation force arises from the synthesized field. We have theoretically and experimentally shown that the synthesized field allows the periodic on/off switching of the acoustic radiation force for one denominational planar standing wave in the straight microfluidic channel. Our study provides a method to temporally manipulate acoustic radiation force. Thus, our theoretical and experimental investigation opens up the possibility of programmable particle and cell manipulations based on the acoustic radiation force without the active controls. This paper has considered only the quantized relative phase, i.e., $\theta_n - \theta_m \in [0, \pi]$, of the field. We expect that the fine-tuned amplitudes and relative phases of the fields increase the flexibility of the temporal manipulation of the acoustic radiation force.

Methods

Figure 7a,b illustrate the measurement setup for the microfluidic channel. Our microfluidic channels (depth = 180 μm, width = 6.41 mm, and length = 32 mm) were manufactured using the standard semiconductor fabrication process. A silicon wafer of 500 μm was etched by the deep reactive ion etching. Following this, the top-side of the silicon wafer was sealed with a glass plate of 700 μm thickness via anodic bonding. The wafer was subsequently diced into small chips, the glass plate was drilled, and the silicon tubes were glued to both edges of the channel. In the next step, piezoelectric transducers (HC-2015S12, Honda Electronics Co., Ltd.) were attached to both the longer sides of the chip, and water containing the small particles was filled in the channel using a piezoelectric micropump (SDMP302, Takasago Fluidic Systems). We used particles of diameter 10.57 μm with 0.11 μm standard deviation (PS-ST-10.6, Microparticles GmbH) at a concentration of 0.05% w/v.

To mimic the ultrasounds emitted from the multiple sources, we applied the synthesized multitone voltage $\sum_{n=1}^{6} V_n \sin(\omega_n t + \eta_n)$ to the piezoelectric elements using an arbitrary waveform generator (Mi2.6021, SPEC-TRUM) with control software (SBench6-Pro 6.1). Thus, the synthesized field was induced in the microfluidic chip. The driving frequency was $\omega_n = \omega_0 + (n-1)\delta\omega$ with $\omega_0/(2\pi) = 117$ kHz and $\delta\omega/(2\pi) = 0.25$ Hz. The power of the waveform generator was amplified with a power amplifier (HSA 2011, NF Corp.). The peak-to-peak voltage at the amplifier output was 40 V. The trajectory of the particles was recorded using an optical microscope (SMZ-10, Nikon Corp.) equipped with a CMOS camera (WRAYCAM-NOA630, WRAYMER Inc.) at a capture rate of 1 Hz. It must also be noted that the channel width was approximately matched to the half-wavelength to create a one-dimensional resonant standing wave.

References

1. King, L. V. On the acoustic radiation pressure on spheres. *Proc. R. Soc. Lond. Ser. A* **147**, 212–240 (1934).
2. Yosioka, K. & Kawasima, Y. Acoustic radiation pressure on a compressible sphere. *Acustica* **5**, 167–173 (1955).
3. Gor'kov, L. P. On the forces acting on a small particle in an acoustical field in an ideal fluid. *Sov. Phys. Dokl.* **6**, 773 (1962).
4. Marzo, A. *et al.* Holographic acoustic elements for manipulation of levitated objects. *Nat. Commun.* **6**, 8661 (2015).
5. Démoré, C. E. M. *et al.* Acoustic tractor beam. *Phys. Rev. Lett.* **112**, 174302 (2014).
6. Fushimi, T., Hill, T. L., Marzo, A. & Drinkwater, B. W. Nonlinear trapping stiffness of mid-air single-axis acoustic levitators. *Appl. Phys. Lett.* **113**, 034102 (2018).
7. Baresch, D., Thomas, J.-L. & Marchiano, R. Observation of a single-beam gradient force acoustical trap for elastic particles: Acoustical tweezers. *Phys. Rev. Lett.* **116**, 024301 (2016).
8. Drinkwater, B. W. A perspective on acoustical tweezers—Devices, forces, and biomedical applications. *Appl. Phys. Lett.* **117**, 180501 (2020).
9. Ochiai, Y., Hoshi, T. & Rekimoto, J. Three-dimensional mid-air acoustic manipulation by ultrasonic phased arrays. *PLoS ONE* **9**, e97590 (2014).
10. Fushimi, T., Marzo, A., Drinkwater, B. W. & Hill, T. L. Acoustophoretic volumetric displays using a fast-moving levitated particle. *Appl. Phys. Lett.* **115**, 064101 (2019).

11. Friend, J. & Yeo, L. Y. Microscale acoustofluidics: Microfluidics driven via acoustics and ultrasonics. *Rev. Mod. Phys.* **83**, 647–704 (2011).
12. Nordin, M. & Laurell, T. Two-hundredfold volume concentration of dilute cell and particle suspensions using chip integrated multistage acoustophoresis. *Lab Chip* **12**, 4610–4616 (2012).
13. Carugo, D. *et al.* A thin-reflector microfluidic resonator for continuous-flow concentration of microorganisms: A new approach to water quality analysis using acoustofluidics. *Lab Chip* **14**, 3830–3842 (2014).
14. Evander, M. & Nilsson, J. Acoustofluidics 20: Applications in acoustic trapping. *Lab Chip* **12**, 4667–4676 (2012).
15. Collins, D. J. *et al.* Two-dimensional single-cell patterning with one cell per well driven by surface acoustic waves. *Nat. Commun.* **6**, 8686 (2015).
16. Petersson, F., Åberg, L., Swärd-Nilsson, A. M. & Laurell, T. Free flow acoustophoresis: microfluidic-based mode of particle and cell separation. *Anal. Chem.* **79**, 5117–5123 (2007).
17. Augustsson, P., Magnusson, C., Nordin, M., Lilja, H. & Laurell, T. Free flow acoustophoresis: Microfluidic-based mode of particle and cell separation. *Anal. Chem.* **84**, 7954–7962 (2012).
18. Ding, X. *et al.* Cell separation using tilted-angle standing surface acoustic waves. *PNAS* **111**, 12992–12997 (2014).
19. Leão-Neto, J. P., Lopes, J. H. & Silva, G. T. Core-shell particles that are unresponsive to acoustic radiation force. *Phys. Rev. Appl.* **6**, 24025 (2016).
20. Silva, G. T. Acoustic radiation force and torque on an absorbing compressible particle in an inviscid fluid. *J. Acoust. Soc. Am.* **136**, 2405–13 (2014).
21. Lima, E. B. & Silva, G. T. Mean acoustic fields exerted on a subwavelength axisymmetric particle. *J. Acoust. Soc. Am.* **150**, 376 (2021).
22. Leão-Neto, J. P. & Silva, G. T. Acoustic radiation force and torque exerted on a small viscoelastic particle in an ideal fluid. *Ultrasonics* **71**, 1–11 (2016).
23. Bruus, H. Acoustofluidics 2: Perturbation theory and ultrasound resonance modes. *Lab Chip* **12**, 20–28 (2012).
24. Bruus, H. Acoustofluidics 7: The acoustic radiation force on small particles. *Lab Chip* **12**, 1014–1021 (2012).
25. Doinikov, A. A., Gerlt, M. S. & Dual, J. Acoustic radiation forces produced by sharp-edge structures in microfluidic systems. *Phys. Rev. Lett.* **124**, 154501 (2020).
26. Collins, D. J. *et al.* Acoustic tweezers via sub-time-of-flight regime surface acoustic waves. *Sci. Adv.* **2**, e1600089 (2016).
27. Wang, Q., Riaud, A., Zhou, J., Gong, Z. & Baudoin, M. Acoustic radiation force on small spheres due to transient acoustic fields. *Phys. Rev. Appl.* **15**, 44034 (2021).
28. Schwarz, T. *Rotation of Particles by Ultrasonic Manipulation*. Thesis (2013).

Author contributions

Competing interests

The authors declare no competing interests.

Additional information

Correspondence and requests for materials should be addressed to H.T.

Reprints and permissions information is available at www.nature.com/reprints.

Publisher's note Springer Nature remains neutral with regard to jurisdictional claims in published maps and institutional affiliations.